Original Article

Model test on support scheme for carbonaceous slate tunnel in high geostress zone at high depth

TAO Zhi-gang[1,2] https://orcid.org/0000-0002-1966-3678; e-mail: taozhigang@cumtb.edu.cn

REN Shu-lin[1,2] https://orcid.org/0000-0003-0408-6246; e-mail: rsl1995@126.com

LI Gan[3]* https://orcid.org/0000-0003-4066-9529; ✉ e-mail: 303521087@qq.com

XU Hao-tian[1,2] https://orcid.org/0000-0003-1012-4632; e-mail: xuhaotian2019@163.com

LUO Sen-lin[1,2] https://orcid.org/0000-0002-2111-3990; e-mail: luosenlin1996@163.com

HE Man-chao[1,2] https://orcid.org/0000-0002-9601-9843; e-mail: 805309740@qq.com

*Corresponding author

1 State Key Laboratory for Geomechanics & Deep Underground Engineering, China University of Mining and Technology, Beijing 100083, China

2 School of Mechanics and Civil Engineering, China University of Mining and Technology, Beijing 100083, China

3 State Key Laboratory of Hydroscience and Engineering, Tsinghua University, Beijing 100084, China

Citation: Tao ZG, Ren SL, Li G, et al. (2021) Model test on support scheme for carbonaceous slate tunnel in high geostress zone at high depth. Journal of Mountain Science 18(3). https://doi.org/10.1007/s11629-020-6509-1

Abstract: The Muzhailing extra-long highway tunnel and corresponding inclined shafts in Lanzhou, Gansu Province, China passes through structurally complex carbonaceous slate that is under high ground stress. Rationally-designed and effective support is of high importance for achieving safe and efficient tunnel construction. The No. 2 inclined shaft of Muzhailing Tunnel was taken as the engineering background prototype, for which, a similar model test was conducted to evaluate the effect of highly pre-tightened constant resistance (NPR, Negative Poisson's Ratio) anchor cable support provision to the geologically complex carbonaceous slate at different depths. Two schemes were proposed during testing: one scheme was without support and the second was with asymmetric support from highly pre-tightened constant resistance anchor cable. Digital speckle displacement analysis system and micro-ground-stress sensors were employed to measure the deformation and shear stress distribution of the tunnel. The results demonstrated that through the second support scheme, the deformation of the surrounding rock could be effectively ameliorated, while this support scheme was applied on the project site of the No.2 inclined shaft, to explore the rationality of the scheme through field engineering tests. On-site monitoring indicated that the deformation of the surrounding rock was within the reasonable design range and the problem of severe tunnel deformation was effectively controlled. The research methods and related conclusions can be used as a reference for the treatment of large deformation problems in deep-buried soft rock tunnels.

Keywords: Tunnel engineering; Support design; Carbonaceous slate; Similar simulation; NPR anchor cable

1   Introduction

Tunnels that are constructed in high depths are often subjected to high geostress and penetrate complex geological structures. Consequently, reasonable support for the surrounding rock is the most important factor to be considered in tunnel design and construction (Oreste et al. 1997; Ortlepp et al. 1998; Miwa et al. 2005; Hisatake et al. 2008; Simona. 2013; Wang et al. 2018; Elizalde et al. 2016; Marinos et al. 2018; Kang et al. 2018.) Muzhailing extra-long highway tunnel and the corresponding inclined shaft penetrate many fault-fractured zones and carbonaceous slate strata. Carbonaceous slate is a complex rock mass, which is commonly found in the southwestern region of China. The corresponding large-scale deformation characteristics and mechanism have been studied by many researchers *(*Chen et al. 2017; Wang et al. 2012). It is prone to high magnitude deformation during tunnel excavation, which would have a major effect on the safety of operations. Taking inclined shaft No. 2 of Muzhailing Tunnel as an example, on-site monitoring results demonstrated the main deformation characteristics as asymmetric deformation, high-magnitude deformation of the surrounding rock, with long duration and severe damage to the initial support structure. Therefore, it was proven as highly important to design effective support, to increase the safety of tunnel excavation.

Many scholars have studied potential support schemes utilizing various methods, including laboratory experiments, numerical simulation and in-situ tests. A rigidly supported scheme (Kimura et al. 1987) was utilized for the Enasan tunnel I in Japan. Reinforced concrete with a thickness of 1.2 m was used for secondary lining, but due to the excessive deformational pressure exerted by the surrounding rock, the steel arch was distorted and fractured, while the secondary lining was severely cracked. Merlini et al. (2018) evaluated the danger of high-magnitude deformation of the highly stressed soft rock in the Ceneri Base extra-long tunnel and proposed a combined support scheme of deformable bracket + anchor net shotcrete + shotcrete reinforced with fibers + steel arch, through which, the subsidence of the tunnel-surrounding rock was effectively controlled. Cao et al. (2018) utilized double-first lining support in Xinchengzi soft rock tunnel along the Lanzhou-Chongqing railway, which was under

high ground stress. Through this method, the deformation was first accommodated and consequently inhibited. This was demonstrated by the research results to be beneficial for the large-scale deformation control of the surrounding rock. Tian et al. (2011) proposed, based on the rheological characteristics of Xiakou soft rock tunnel, a support scheme that included the addition of U-steel compressible stents and foam concrete filling layers to a spray anchor network was utilized. Through this scheme, a stable supporting force suitable for the long-term stability preservation of the tunnel was found to be provided. Zhang et al. (2014) studied multiple support measures, including a steel grid and a steel frame. It was discovered that the stress of the initial supporting steel framework could finally be effectively controlled and an optimized supporting effect could be obtained.

The aforementioned research studies demonstrated that two important features were required for effective support structures in high-stress soft rock tunnel engineering works. Subsequently, on the one hand, the effective support structures would provide sufficient flexibility for the tunnel to adapt to the deformation of the surrounding rock, whereas on the other hand, sufficient rigidity would be supplied to prevent high-magnitude rock mass deformation. A type of anchor cable with constant resistance and large deformation magnitude called an NPR (Negative Poisson's Ratio) anchor cable was therefore developed by Manchao He. This anchor cable has become popular and achieved good application results in the field of soft rock support in coal mines, but it has received insignificant amounts of investigation in the field of tunnel engineering (He et al. 2014).

In the present work, considering the asymmetric deformation characteristics of the surrounding rock after excavation within inclined rock strata, an asymmetric coupling support strategy was proposed, within which, the effects of highly pre-tightened constant resistance anchor cable support (NPR anchor cable) at a carbonaceous slate tunnel under different depths were studied through similar physical model tests, with a digital speckle displacement analysis system utilization. The contact stress measurement method was utilized to study the variations in the displacement field and surrounding-rock deformation. The feasibility of NPR anchor cable support was consequently verified through the corresponding application within a practical engineering context.

2 Engineering Background

The Muzhailing extra-long highway tunnel and corresponding inclined shafts in Lanzhou, Gansu province, China penetrated structurally complex carbonaceous slate that was under high ground stress (Fig.1). The original support scheme for the rock surrounding was to install self-propelled hollow grouting ancho rs, low-sized circumferential grouted ducts and steel mesh (Fig.2). A three-bench excavation sequence was adopted, signifying upper-bench excavation, followed by middle-bench excavation and finally bottom-bench excavation. However, during the construction of the project, the initial support failure occurred many times, while the corresponding project deformation characteristics were mainly manifested as asymmetric deformation, high deformation of the surrounding rock and long deformation duration. Therefore, the original support method was required to be modified for optimal effectiveness. The No. 2 inclined shaft of Muzhailing tunnel was utilized as an example to study the reasonable support scheme.

The No. 2 inclined shaft was located in the middle of the main tunnel (Fig.1), the starting point was K0 + 000 and the ending point was K1 + 813, while the total length was 1813 m. The maximum depth was 591 m, on the basis of as a high depth tunnel. The surrounding rock was mainly composed of carbonaceous slate inclined at angles with respect to the horizontal that ranged from 30° to 85°. In-situ survey and tests on laboratory specimens were utilized to obtain values for the physical and mechanical parameters of the real rock. These parameters are listed in Table 1. The geostress of the rock surrounding inclined shaft No. 2 was 15.7 MPa and the maximum horizontal principal stress was 24.95 MPa (Fig.3); the inclined shaft could be therefore classified as an extremely high geostress tunnel according to the Standard for Engineering Classification of Rock Mass (GB/50218-94). The
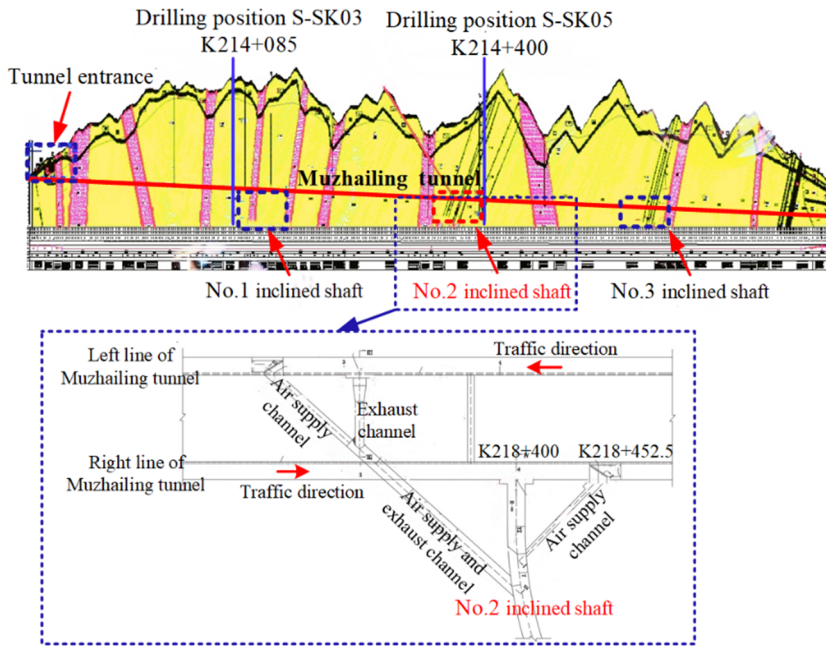

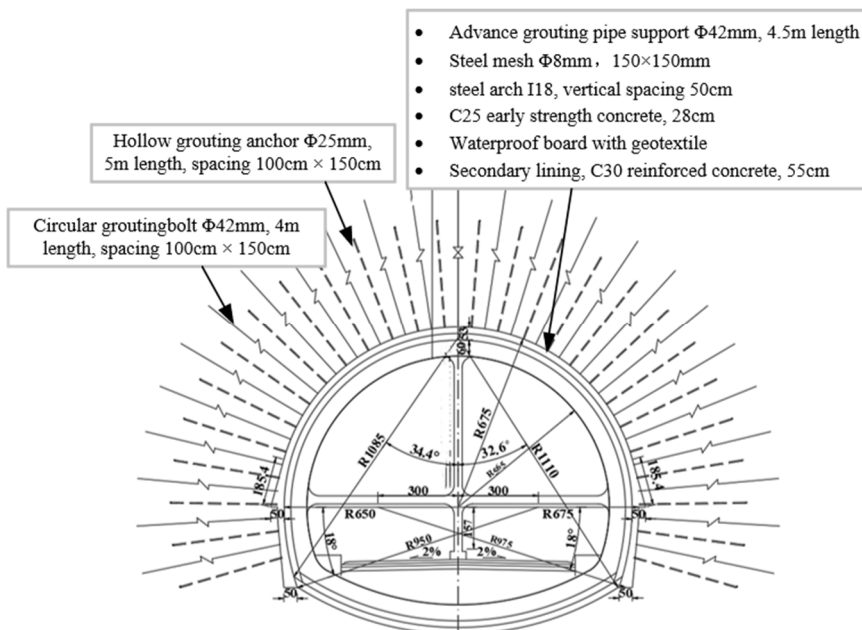**Fig. 1** Geological profile of Muzhailing tunnel.

Fig. 2 Original support scheme.

surrounding rock of the inclined shaft sustained severe deformation through the original support scheme utilization, as presented in Figs.4(a) ~ 4(c), within which, the severe deformation of the surrounding rock and primary lining and the distortion of steel arches were visible. The surrounding rock deformation was regarded as the partition standard, while the inclined shaft was divided into four areas from the entrance to K1713 m, which were divided into basically stable area (lower than 100 mm), slight deformation area (100~250 mm), high deformation area (250~1000 mm) and severe deformation area (exceeding 1000 mm). The specific description is presented in Fig.5.

3 Physical Model Testing

3.1 Law of similarity

A similar physical model was an effective means, through which, the research of complex geotechnical engineering problems was more economical and efficient, compared to the field experiments and in-situ tests. Therefore, such research is currently widely utilized in contexts, such as in roadway engineering works (Wang et al. 2018; Sun et al. 2017, 2018; Gong et al. 2013, 2015; Li et al. 2013, 2015; He 2011), tunnel engineering works (Rui et al. 2019; Zhang et al. 2018; Lin et al. 2015; Jeon et al. 2004) and slope engineering works (Kulasingam et al. 2004; Zhang et al. 2007; Lin et al. 2015; Khorasani et al. 2019). Through previous studies, it has been established that similar models must satisfy a series of similarity requirements such as geometry, physico-mechanical properties, boundary conditions and initial stress conditions. Many similarity constants were required to be determined to simulate the practical geotechnical engineering environment precisely. The main physical similarity constants were as follows. In this case, the subscript 'p' represents the prototype and 'm' represents the test model.

$$C_L = \frac{L_p}{L_m} ; C_\sigma = \frac{\sigma_p}{\sigma_m} ; C_E = \frac{E_p}{E_m} ; C_\gamma = \frac{\gamma_p}{\gamma_m} ; C_\upsilon = \frac{\upsilon_p}{\upsilon_m} \quad (1)$$

where C_L is the geometric dimension similarity constant, C_σ is the stress similarity constant, C_E is the elastic modulus similarity constant, C_γ is the body
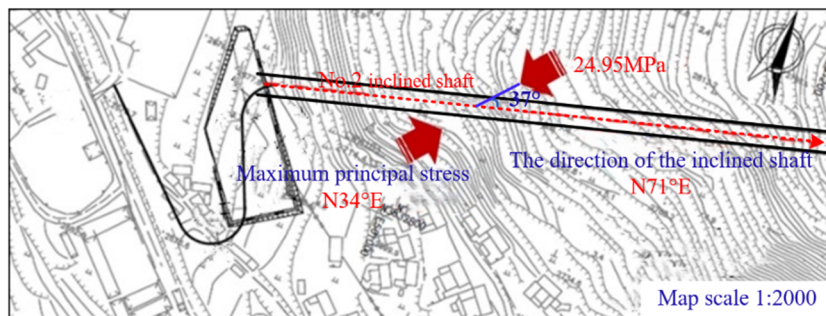
Fig. 3 No.2 inclined shaft and maximum horizontal principal stress.

Fig. 4 Failure characteristics of rock surrounding of No.2 inclined shaft.

Table 1 Mechanical and material properties of Carbonaceous slate

Types	Volumetric weight (kN/m³)	Compressive strength (MPa)	Elastic modulus (GPa)	Poisson ratio	Friction angle (°)
Real rock	24.60	29.5	6.30	0.21	26
Artificial rock	14.47	1.0	0.22	0.21	26

Buried depth: 35-137m
Footage: 60-250m
Vault sedimentation: 120-180mm
Peripheral convergence: 150-230mm

Buried depth: 568-591m
Footage: 525-564m
Vault sedimentation: 240-565mm
Peripheral convergence: 637-3145mm
Maximum deformation speed: 831mm/d

Buried depth: 280-290m
Footage: 764-865m
Vault sedimentation: 250-427mm
Peripheral convergence: 320-600mm

Buried depth: 447-517m
Footage: 1280-1480m
Vault sedimentation: 215-308mm
Peripheral convergence: 236-553mm

No.2 inclined shaft entrance

Maximum burial depth: 591m

Footage :1713m

0m 120m 240m 360m 480m 600m 720m 840m 960m 1080m 1200m 1320m 1440m 1560m 1680m 1800m

Buried depth: 137-215m
Footage: 250-410m
Vault sedimentation: 230-327mm
Peripheral convergence: 300-580mm

Buried depth: 548-569m
Footage: 622-666m
Vault sedimentation: 140-458mm
Peripheral convergence: 127-2936mm
Maximum deformation speed: 814mm/d

Buried depth: 300-376m
Footage: 1050-1200m
Vault sedimentation: 236-415mm
Peripheral convergence: 270-450mm

Buried depth: 526-582m
Footage: 1510-1713m
Vault sedimentation: 310-411mm
Peripheral convergence: 220-1200mm

Basically stable area: deformation amount ＜100mm, total length 407m

Slight deformation area: deformation amount 100-250mm, total length 250m

Large deformation area: deformation amount 250-1000mm, total length 717m

Severe deformation area: deformation amount ＞1000mm, total length 338m

Fig. 5 Deformation zoning of surrounding rock of No.2 inclined shaft.

force similarity constant and C_v is the Poisson's ratio similarity constant, L is the geometric dimension, σ is the stress, E is the elastic modulus, γ is the body force, v is the Poisson's ratio.
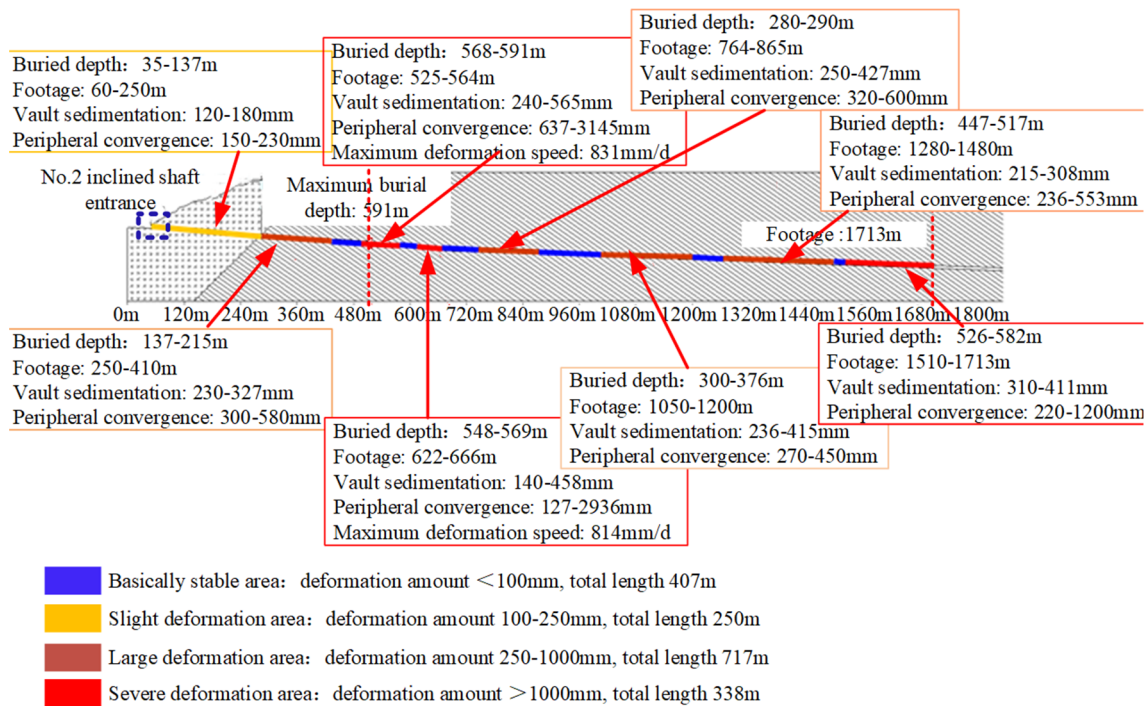
Moreover, the model and prototype should satisfy the differential equations of equilibrium:

$$\left(\sigma_{ij,i}\right)_p + \left(f_j\right)_p = 0 \tag{2}$$

$$\left(\sigma_{ij,i}\right)_p = \left(\frac{\partial \sigma_{1j}}{\partial x_1}\right)_p + \left(\frac{\partial \sigma_{2j}}{\partial x_2}\right)_p + \left(\frac{\partial \sigma_{3j}}{\partial x_3}\right)_p \tag{3}$$

$$\left(\sigma_{ij,i}\right)_m + \left(f_j\right)_m = 0 \tag{4}$$

$$\left(\sigma_{ij,i}\right)_m = \left(\frac{\partial \sigma_{1j}}{\partial x_1}\right)_m + \left(\frac{\partial \sigma_{2j}}{\partial x_2}\right)_m + \left(\frac{\partial \sigma_{3j}}{\partial x_3}\right)_m \tag{5}$$

In addition, the stress, strain, elastic modulus and Poisson's ratio of the model and prototype must satisfy the following equations:

$$\left(\varepsilon_{ij}\right)_p = \left(\frac{1+\upsilon_p}{E_P}\right)\left(\sigma_{ij}\right)_p - \frac{\upsilon_p}{E_P}\left(\sigma_{kk}\delta_{ij}\right)_p \tag{6}$$

$$\left(\varepsilon_{ij}\right)_m = \left(\frac{1+\upsilon_m}{E_m}\right)\left(\sigma_{ij}\right)_m - \frac{\upsilon_m}{E_m}\left(\sigma_{kk}\delta_{ij}\right)_m \tag{7}$$

where $\sigma_{ij,i}$ is the component of stress in the x, y, and z axes, f_j is the component of per unit volume force in the x, y, and z axes, $i = 1, 2, 3, j = 1, 2, 3$.

Finally, the general law of similarity between the prototype and model could be deduced as:

$$C_\sigma = C_L \cdot C_\gamma; C_E = C_L \cdot C_\gamma \tag{8}$$

3.2 Build of physical model

In order to simulate the studied tunnel, the "Physically Finite Elemental Slab Assemblage" (PFESA) (He 2011) was utilized to construct the 30°-inclined rock strata of the geological physical model at the State Key Laboratory for Geomechanics and Deep Underground Engineering at the China University of Mining and Technology, Beijing (CUMTB). A model material was developed to satisfy the requirements of the scaled testing, comprising a mixture of barite powder, quartz powder, plaster, talcum powder and water. The adopted mixing ratio was:

Barite powder: quartz powder: plaster: talcum powder: water = 0.495: 0.150: 0.085: 0.080: 0.190.

The physical-mechanical parameters of the artificial rock are listed in Table 1. We calculate that C_σ is 29.5, C_E is 29.5, and C_γ is 1.7.

The main components of the model test facility, as presented in Fig. 6a, were the experimental platform, hydraulic loading system and hydraulic control system. The dimensions of the model test system were 3310×3010×970 mm³, while the
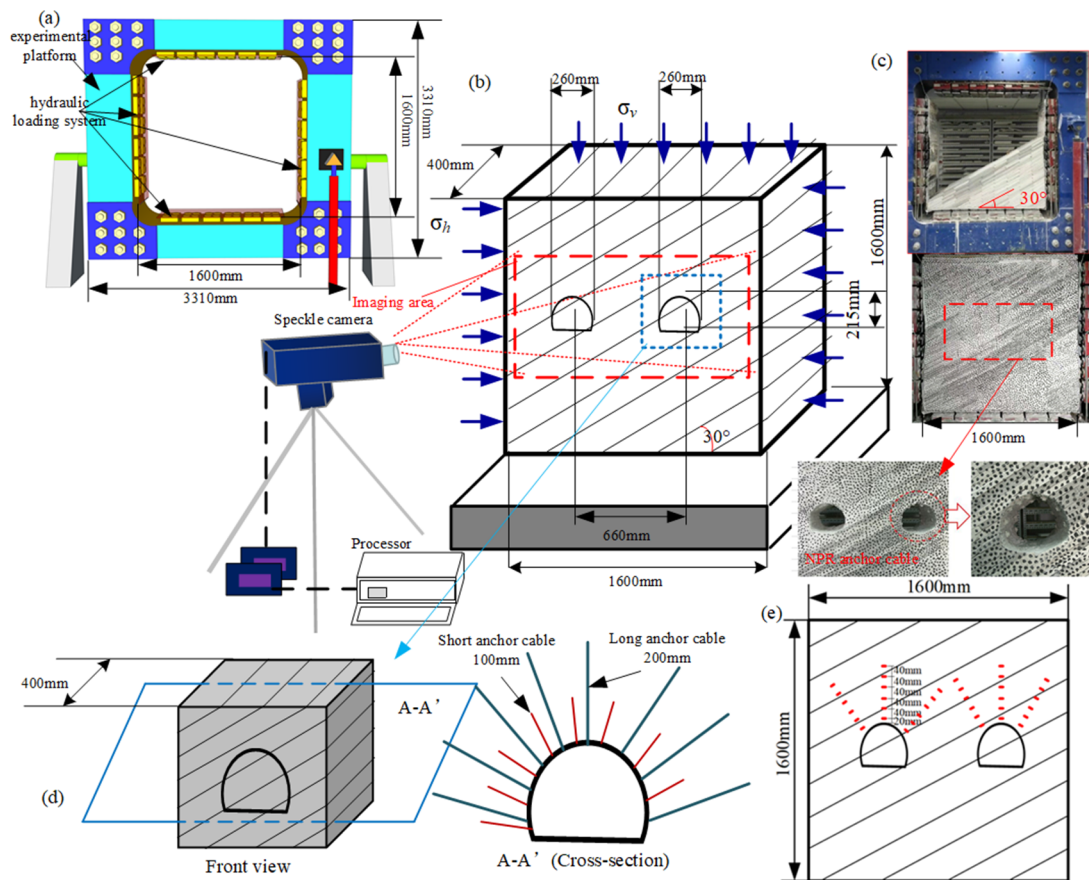
Fig.6 Constructed similar simulation model. (a) Schematic diagram of model test facility; (b) Schematic diagram of model; (c) Photograph showing of laboratory model overview; (d) A tunnel supported with NPR (Negative Poisson's Ratio) anchor cable and cross-section view (A-A'), (e) Layout of stress sensors.

maximum size of the PFESA model was 1600×1600×400 mm³. All elementary slabs were fabricated with the same surface dimensions, 400×400 mm² and a thickness of 3 mm. According to the geometric dimensions of the simulation prototype and of the laboratory equipment, 50 was selected as the geometric dimension similarity constant, C_L. In this study, two model tests were performed under each overburden depth, to investigate the deformation and analyze the stress of the tunnel:

(1) Test 1: deformation and stress analysis of a tunnel without any support.

(2) Test 2: deformation and stress analysis of a tunnel supported with NPR anchor cables.

In order to more vividly reduce experiment costs and compare the deformation characteristics of tunnels under different supporting conditions, the two tunnel-support schemes were installed side-by-side in each PFESA model. Since the present study was focused on deformation and stress investigation inside the tunnel under different overburden depths,

the effects of excavation process were not considered. After the overall model was built, the tunnel outline was drawn within the area to be excavated, while consequently electric drills and other equipment were utilized for tunnel excavation. After the excavation was completed, the main follow-up research work was carried out. The model prototype monitoring indicated that it sustained significant asymmetric deformation that was highest on the left side of the tunnel. Consequently, an asymmetric NPR anchor cable was proposed in this study. The similar simulation model constructed for this test is presented in Fig. 6.

The high-pre-tightening constant resistance anchor cable (NPR anchor cable) support, which demonstrated ultra-high energy-absorbing capacity and extraordinarily high elongation at high constant resistance, was developed by Manchao He (He et al. 2014). The NPR anchor cable consisted of a casing pipe, a piston-shaped cone body within the casing pipe, an ordinary anchor cable installed on the cone

body, a face pallet and a locking device (Fig. 7) (He et al. 2014). The diameter of the narrower end of the constant-resistance body was slightly smaller than the inner diameter of the casing pipe, while the diameter of the wider end was 2 mm larger than the inner diameter of the casing pipe. When the constant resistance body slid within the constant-resistance casing pipe, it produced radial expansion deformation, resulting in a negative Poisson's ratio structural effect. The working principle could be briefly outlined as follows:

(a) Elastic deformation stage: the deformation of the tunnel-surrounding rock was applied to the anchor cable through the face pallet and the internal fixed section. When the deformation energy of the surrounding rock was low-sized and the axial force on the anchor cable was lower than the designed constant resistance force of the NPR anchor cable, the constant resistance device did not function, while the NPR anchor cable functioned on elastic deformation of the ordinary anchor cable to resist rock deformation and failure (Fig. 7a).

(b) Structural deformation stage: with the accumulation of surrounding rock deformation, the axial force on the anchor cable was higher than or equal to the designed constant resistance force of the NPR anchor cable. Friction sliding of the constant resistance body along the inner wall of the casing pipe occurred. During sliding phase, constant resistance was maintained. Rock mass deformation and failure was resisted by the structural deformation of the constant resistance device (Fig. 7b).

(c) Extreme deformation stage: Fig. 7c presents the working state for the NPR anchor cable at full elongation while rock mass deformation was retained.

The NPR anchor cable was required to be shrunk for use in the similar model test and this was accomplished with 3D printing technology. The parameter values of the reduced NPR anchor cable were established through reference to previous research results, which are presented in Table 2. The miniaturized NPR anchor cable model is presented in Fig. 8a. In order to explore whether the miniature NPR anchor cable model met the experimental requirements or not, static tensile testing was carried out with a tensile testing machine. The maximum tensile force of the machine was 500 N and the corresponding maximum test range was 250 mm. A constant loading rate of 1 mm/min was adopted for tensile loading. Five examples of the constant-

resistance anchor cable models were tested for the loading experiment, after which, the experimental results are presented in Fig.8b. The miniature NPR anchor cables first sustained elastic deformation, for which, the relationship between displacement and
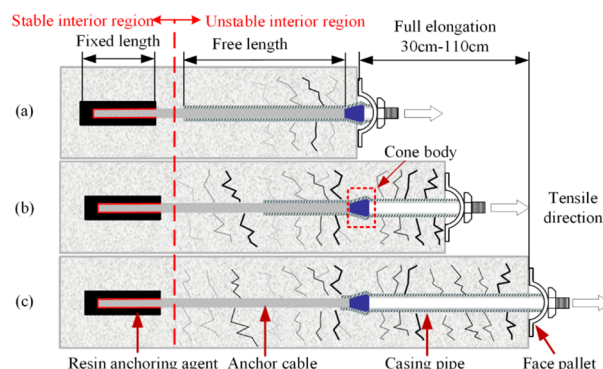

Fig.7 Working principle of NPR (Negative Poisson's Ratio) anchor cable (He et al. 2014).

Table 2 Main physical parameters of miniaturized cable model

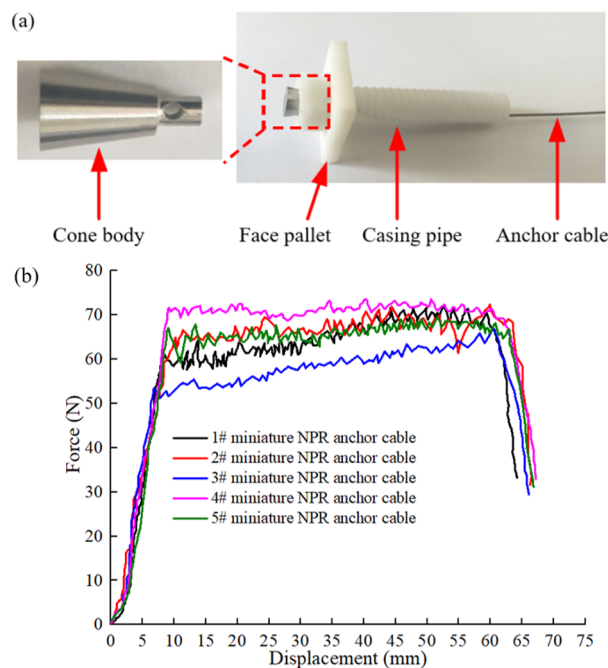| Parameters	Value
Length of the sleeve (mm)	60
Outer diameter of the sleeve (mm)	10
Inner diameter of the sleeve (mm)	8
Narrow-end diameter of the cone (mm)	5
Wide-end diameter of the cone (mm)	8.2
Length of the cone (mm)	10

Fig. 8 Miniature NPR anchor cables (a) Diagram of miniature NPR (Negative Poisson's Ratio) anchor cables (b) Force-displacement curves.

stress was basically in accordance with the law of Hooke. Subsequently, the cables entered the stage of constant resistance deformation, while a constant resistance force between 53 N and 70 N was maintained over a displacement length of between 50 mm and 54 mm. The force-deformation curves of the miniature NPR anchor cables were in good agreement with the curves of the actual constant resistance anchor cable, demonstrating good constant-resistance characteristics. It could therefore be concluded that the miniature anchor cable met the experimental requirements.

A digital speckle measurement and analysis system (Ma et al. 2002) with digital image correlation (DIC) method, provided non-destructive, non-contact and real-time testing to observe the physical step of material deformation and displacement. The avoidance of surface contact had the advantage of influence minimization of human factors on the experiment. The corresponding basic principle was to obtain a speckle field with a high-speed camera and the subsequent speckle displacement calculation to obtain the deformation field. The main components of the system were a light source, a high-speed camera and processing software. The distribution and development of shear stresses around the tunnel were measured with micro-ground-stress sensors arranged in the upper left corner, top and upper right corner of the tunnel, with sensors located at 2 cm, 6 cm, 10 cm, 14 cm, 18 cm and 22 cm afar from the tunnel surface at each location, as presented in Fig. 6e.
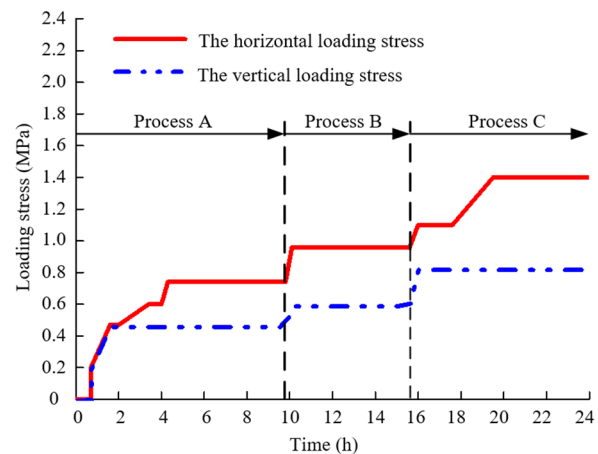
3.3 Model testing scheme

The model testing system was equipped with a hydraulic servo system that could impose a uniformly distributed load on the top and two side boundaries of the model. The bottom of the model was constrained during testing and subsequently a rigid boundary condition was simulated. The vertical and horizontal stresses under different burial depths were obtained through geological survey data analysis, while the model loading scheme was calculated through the application of stress similarity ratio. The incremental

pressure method was adopted in the model test, during which, each pressure increment being 0.2 MPa. The overall test was divided into three steps. Step A was to load with geostress to simulate a burial depth of 250 m. During this step, the horizontal stress was loaded through four increments to reach 0.8 MPa and the vertical stress was loaded through two increments to reach 0.4 MPa, whereas consequently the pressure was retained stable for 6 h. In step B, additional geostress was loaded to simulate a burial depth of 350 m. One further increment of horizontal stress and vertical stress was added, while the pressure was again retained stable for 6 h. In step C, geostress load was added to simulate a burial depth of 500 m. Two additional increments of horizontal stress were added to reach 1.4 MPa, while one further increment of vertical stress was added to reach 0.8 MPa. The loading scheme is presented in Table 3, while the loading curve is presented in Fig.9.

Fig. 9 Loading scheme for model test.

4 Results and Discussion

4.1 Tunnel deformation analysis

(1) Step A

The deformation characteristics of the tunnel at the end of step A, through which, a burial depth of 250 m was simulated, are presented in Fig.10a, the

Table 3 Physical model loading scheme

| Buried depth	250 m		350 m		500 m	
Stress types	Vertical stress	Horizontal stress	Vertical stress	Horizontal stress	Vertical stress	Horizontal stress
Prototype (MPa)	7.00	11.00	9.00	14. 5.	12.5.	21.00
Physical model (MPa)	0.47	0.74	0.60	0.96	0.83	1.40

tunnel without support was at the left side, while with NPR anchor cable support the deformation on the right. Even though no displacement of the surrounding rock was visible in the model photograph with the naked eye, the digital speckle measurement and analysis system did reveal certain amount of displacement. The rock surrounding the tunnel without any support sustained a maximum displacement of 1.665 mm at the left top corner of the tunnel. The tunnel with NPR anchor cable support had a maximum displacement of 1.58 mm on the left side and of 0.74 mm on the right side. Due to the shallow burial depth of the tunnels, the tunnels did not sustain pronounced deformation and dam age, either with NPR anchor cables or without.

    (2) Step B

As presented in Fig.10b, high amount of deformation occurred on the left and right sides of the tunnel without support during step B. Cracking occurred on the left side of the tunnel near the free surface. However, speckles in the area where this cracking occurred could not be easily identified, due to the shedding of speckle points. The widest crack was 2.2 mm wide (measured with Vernier caliper). In addition, block slipping occurred on the right side of the tunnel, with a maximum displacement of 0.96 mm. On the other hand, the rock surrounding the tunnel supported by NPR anchor cable demonstrated non-apparent fracture.

(3) Step C

The deformation characteristics of the unsupported tunnel could be divided into three stages, as presented in Fig.10c ~ 10e. Firstly, the separated layer on the left side of the tunnel became further developed, while slipping occurred on the right side of the tunnel. The cracking on the le ft side consequently continued to expand upwards, while stripping occurred at the left top corner of the tunnel. Finally, the surrounding rock on the left side of the tunnel was severely damaged and collapse occurred. The deformation and destruction of the tunnel consequently stopped. The displacement of both sides
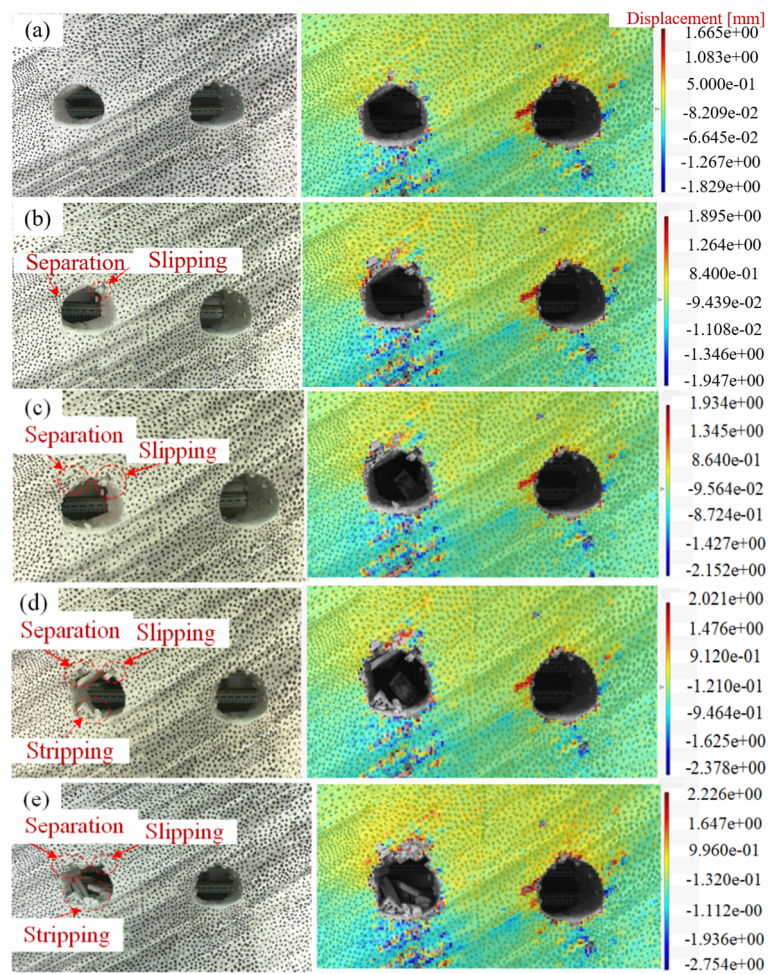
Fig. 10 Experimental images (Model photographs at left of images and speckle displacement image in the right). (a) step A (b) step B (c)~(e) step C

of the tunnel with NPR anchor cable support also increased significantly; the highest displacement was 2.226 mm and occurred at the left side of the tunnel. However, no apparent damage occurred.

The three steps of the experiment clearly demonstrated a significantly higher magnitude of deformation at the left side of the tunnel than in other parts and that the NPR anchor cable was effectively able to control the deformation of the rock surrounding the tunnel.

4.2 Shear stress analysis of tunnel-surrounding rock

(1) Step A

The monitoring results (Fig.11) demonstrated that the simulated unsupported tunnel at a depth of 250 m sustained maximum shear stress at 2 cm from

the tunnel free surface (excavation boundary), while the shear stress was higher at the left spandrel of the tunnel than at the vault and right spandrel of the tunnel. As the distance to the tunnel surface increased, the stress on the left side, the vault and right side of the tunnel gradually decreased, indicating that under this condition, the tangential stress of the surrounding rock was mainly concentrated at the edge of the rock surrounding the tunnel and that the range of the plastic zone was relatively low.

Fig.12 presents the results for a tunnel at the same depth, but it provided with an asymmetric constant resistance anchor cable support. The maximum shear stress of the surrounding rock was

again recorded close to the free surface of the tunnel, while the shear stress gradually decreased with distance from the free surface of the tunnel. The stress changes at different locations in the surrounding rock were similar to the changes inside the unsupported tunnel, mainly due to the shallow depth of the tunnel (250 m), which caused the deformation of the surrounding rock to become low and the effect of the NPR anchor cable to be apparent.

(2) Step B

In step B of the experiment, loading was continued until the simulated depth of the tunnel gradually reached 350 m. As presented in Fig.13, in the tunnel without support the tangential stress at a
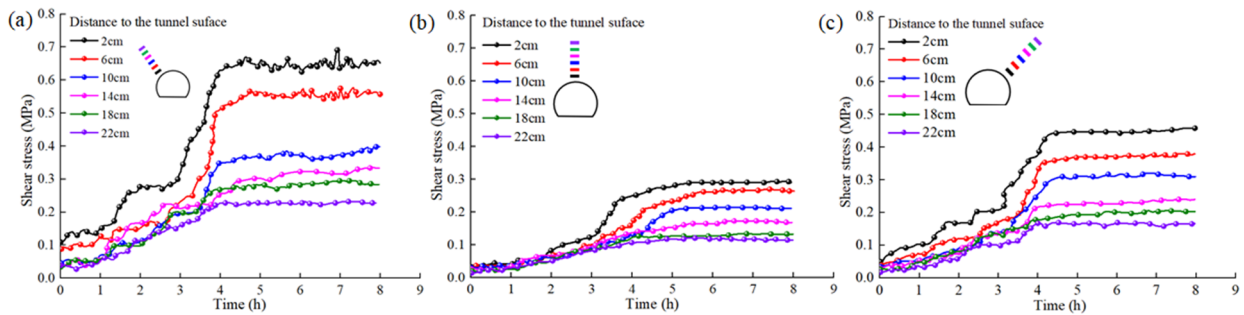

Fig. 11 Shear stress monitoring results of a tunnel without support at 250 m depth. (a) Left shoulder of the tunnel; (b) top of the tunnel; (c) right shoulder of the tunnel.
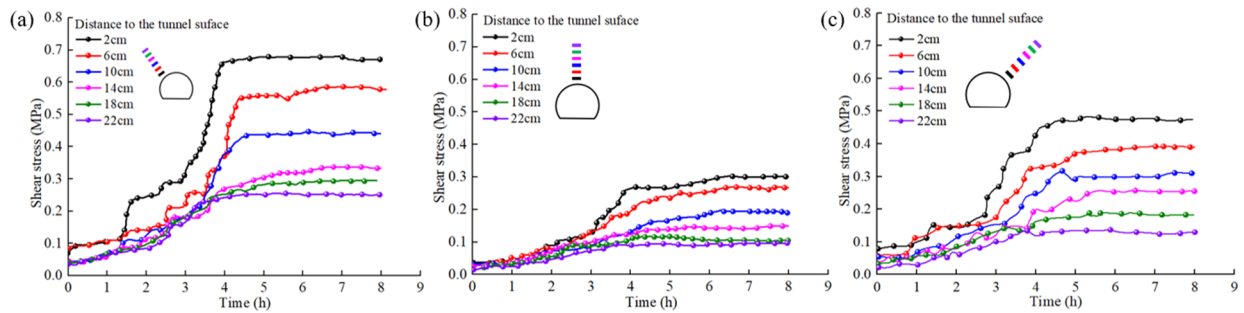

Fig. 12 Shear stress monitoring results of a tunnel with NPR anchor cable support at 250 m depth. (a) Left shoulder of the tunnel; (b) top of the tunnel; (c) right shoulder of the tunnel.
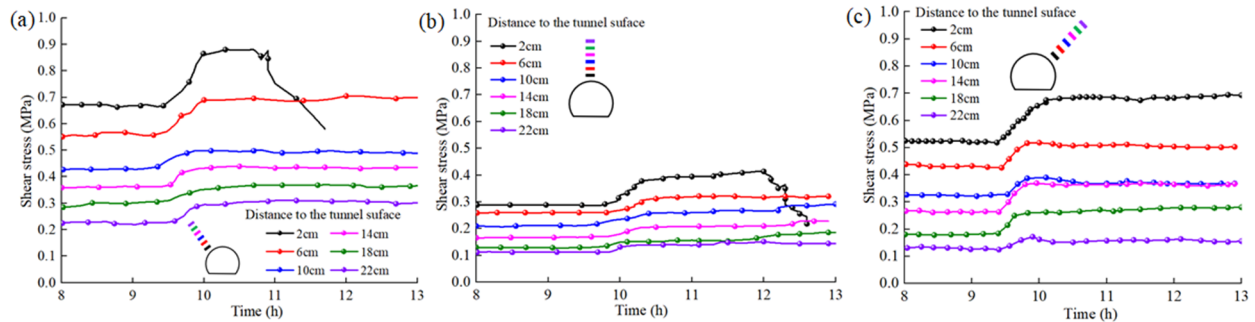

Fig. 13 Shear stress monitoring results of a tunnel without support at 350 m depth. (a) Left shoulder of the tunnel; (b) top of the tunnel; (c) right shoulder of the tunnel.

distance of 2 cm from the surface of the left spandrel of the tunnel increased to 0.88 MPa and subsequently dropped sharply, mainly due to the destruction of the tunnel edge at this time frame, which signified that the surrounding rock pressure could not be transmitted to the stress sensors. However, no steep drop occurred at 6 cm from the free surface, indicating that the damaged area did not reach a high depth inside the surrounding rock. Normal monitoring results were returned for stress at the vault and right spandrel of the tunnel, as the tunnel was not damaged in these areas.

The results of the monitoring points at the left spandrel, vault and right spandrel of the tunnel of the NPR anchor cable-supported tunnel (Fig.14) demonstrated that the maximum shear stress was again reached at 2 cm, afar from the free surface in the left side of the tunnel, increasing to approximately 0.9 MPa, but no damage occurred.

(3) Step C

As presented in Fig.15, as the simulated burial depth was increased to 500 m, the shear stress at a distance of 6 cm from the excavation surface at the left spandrel of the tunnel with no support reached 0.93 MPa, followed by an abrupt drop in the pressure value. Moreover, at a distance of 10 cm from the

tunnel surface, the shear stress was still gradually increasing, consequently indicating that the area of the surrounding rock that failed on the left side of the tunnel had developed to a distance of approximately 6 cm from the left shoulder surface of the tunnel. At a distance of 6 cm from the excavation surface at the vault of the tunnel, the tangential stress reached 0.45 MPa and suddenly dropped, whereas normal monitoring stress results were obtained from 10 cm of the surface, indicating that the area damaged at the top of the tunnel had reached 6 cm from the initial free surface. The shear stress at the right side of the tunnel presented a normal increase, indicating that insignificant damage occurred at that area.

Fig.16 presents that the shear stress at each position of the tunnel supported with NPR anchor cable increased gradually as the stress gradient increased. The maximum shear stress at the left side of the tunnel reached 1.6 MPa, while at the top of the tunnel it reached 0.5 MPa and at the right side of the tunnel it reached 0.92 MPa. However, the tunnel did not sustain significant deformation.

According to the aforementioned monitoring results, it c ould be concluded that under the same loading pressure, the NPR anchor cable was able to increase the shear resistance of the surrounding rock
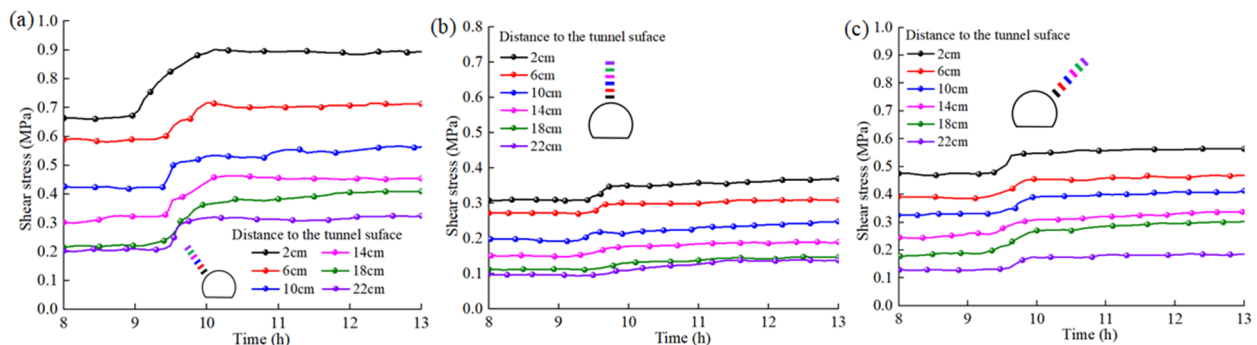

Fig. 14 Shear stress monitoring results of a tunnel with NPR anchor cable support at 350 m depth. (a) Left shoulder of the tunnel; (b) top of the tunnel; (c) right shoulder of the tunnel.
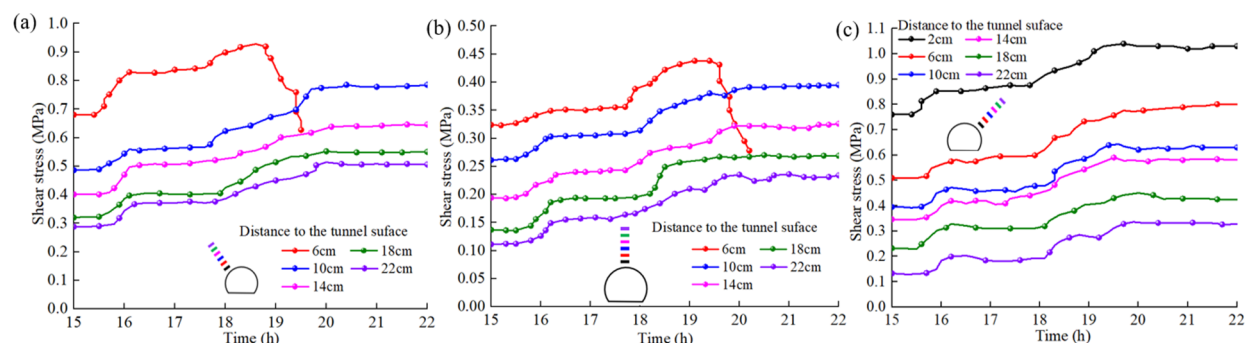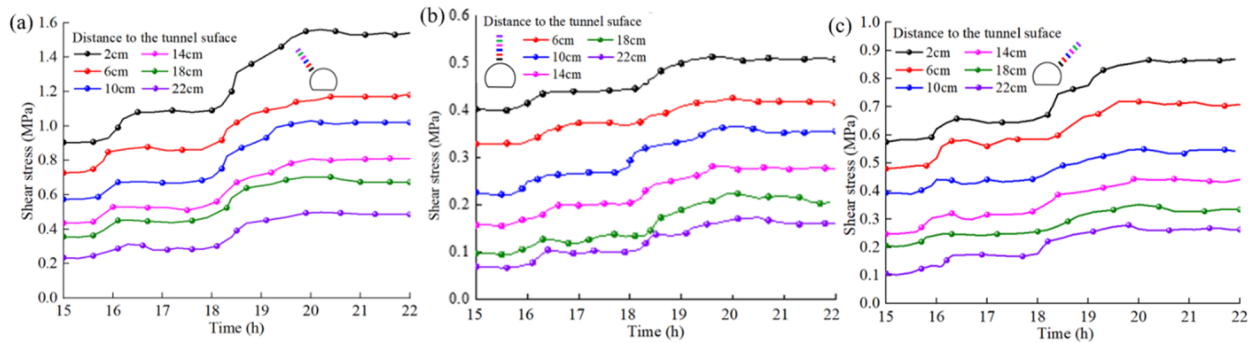

Fig. 15 Shear stress monitoring results of a tunnel without support at 500 m depth. (a) Left shoulder of the tunnel; (b) top of the tunnel; (c) right shoulder of the tunnel.

Fig. 16 Shear stress monitoring results of a tunnel with NPR anchor cable support at 500 m depth. (a) Left shoulder of the tunnel; (b) top of the tunnel; (c) right shoulder of the tunnel.

Table 4 Parameter design for NPR (Negative Poisson's Ratio) anchor cable support scheme at No.2 inclined shaft

Location	Technical parameters	Section design
Upper bench excavation	(1) NPR anchor cable: L=5300 mm, P≥350 kN, B=1000×600 mm. (2) NPR anchor cable: L=10300 mm, P≥350 kN, B=2000×1200 mm. (3) NPR anchor reinforcement support: Two additional NPR cables in the upper left corner of the tunnel, P≥30 kN, B=1000×1200 mm. (4) Steel mesh: D=8 mm, M=100×100 mm. (5) Concrete: H=100 mm.	
Middle bench excavation	(1) NPR anchor cable: L=5300 mm, P≥350 kN, B=1000×600 mm. (2) NPR anchor cable: L=10300 mm, P≥350 kN, B=2000×1200 mm. (3) NPR anchor reinforcement support: Two additional NPR cables in the upper left corner of the tunnel, P≥30 kN, B=1000×1200 mm. (4) Steel mesh: D=8 mm, M=100×100 mm. (5) Concrete: H=100 mm.	
Bottom bench excavation	(1) NPR anchor cable: L=5300 mm, P≥350 kN, B=1000×600 mm. (2) NPR anchor cable: L=10300 mm, P≥350 kN, B=2000×1200 mm. (3) Steel mesh: D=8 mm, M=100×100 mm. (4) Steel arch: Spacing distance 1200 mm, erected between 5300 mm NPR anchor steel strips, interleaved with 10300 mm NPR anchors. (5) Concrete: H=100 mm.	

Notes: L - NPR anchor cable length (mm); P – Prestress (kN); B – Spacing (mm); D - Diameter of mesh reinforcement (mm); M - Steel mesh size (mm); H - Initial spray thickness of concrete (mm).

and effectively control the surrounding rock failure. A combination of long and short NPR anchor cables is commonly used to support layered surrounding rock in practical applications. The short anchor cables can connect several rock layers together and increase the friction between rock layers. From the viewpoint of structural mechanics, this forms a "combined beam" structure, which significantly reduces internal stress and deflection. The long anchor cables mainly play the role of "suspension", linking the "composite beam" structure with the stabilized surrounding rock and significantly improve the surrounding rock stability.

5 Engineering Application

A new support scheme was proposed according to the study results of the similar model tests, within which, the tunnel was supported with asymmetric NPR anchor cables, as described in Table 4. In addition, a field engineering test was conducted on the project site of the No.2 inclined shaft. In order to control the experimental variables, the area in the K1738 – K1813, which was similar to the increased depth and surrounding rock condition of the severely
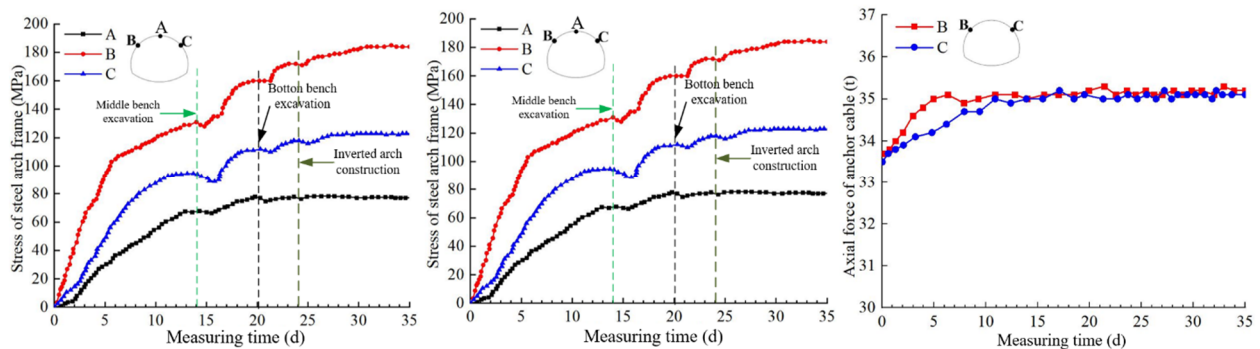
Fig. 17 Field test results. (a) Time-history curve of surrounding rock displacement; (b) time-history curve of steel arch internal force; (c) Time-history curve of anchor cable force.

deformed tunnel under the original support scheme, was selected. For a comprehensive analysis of the effect of the new support scheme, seven monitoring sections, the K1765 to K1795, were designed. The distance along each section was 5 meters and the depth of the tunnel was approximately 500 m. Five displacement monitoring points were set for each section: inside the vault, the left spandrel, the right spandrel, the left arch waist and the right arch waist. Stress monitoring points for the steel arches were also set inside the vault, the left spandrel and the right spandrel of each section. In addition, two anchor cable stress-monitoring points were set at the left and right spandrels, respectively. In the present work, the monitoring results for cross-section K1790 were taken as the example for analysis, as presented in Fig.17.

All monitoring sections were located below 500 m of the overburden. It should be noted that after the NPR anchor cable asymmetric support scheme adoption, the deformation stabilization of the tunnel section walls generally occurred within 25 to 30 days, while the data did not fluctuate in the subsequent results. Therefore, only the monitoring data of the previous 35 days were displayed. According to the monitoring results in Fig.17a, the deformation of the left spandrel was higher than of the right side and vault of the tunnel, while the maximum deformation of the left spandrel was 230 mm. The deformation rate of the surrounding rock reached a maximum after upper bench excavation, while deformation gradually stopped after the inverted arch construction completion. Less than 500 mm of deformation convergence occurred in any one section, which was lower than the design value and within the controllable range. As presented with the stress-monitoring results for the steel arch in Fig. 17b, the
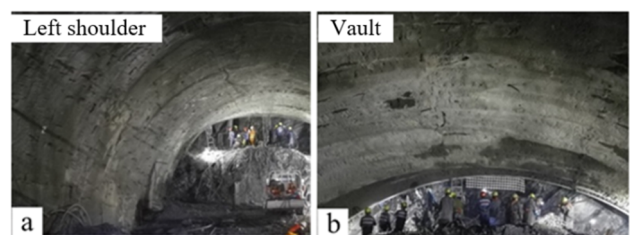
Fig. 18 Supporting effect diagram of NPR (Negative Poisson's Ratio) support scheme (a) left shoulder of tunnel (b) vault of tunnel.

stress value was highest on the left spandrel, but it did not reach the yield strength. In addition, due to the deformation of the surrounding rock, the axial force of the NPR anchor cable initially increased linearly and subsequently reached the constant resistance value. Due to the inherent properties of the constant resistance anchor cable, the force of the anchor cable was always maintained at approximately 35 t (Fig. 17b). In the K1613–K1713 section of the tunnel, the ratio of steel arch replacement was 40% prior to the implementation of the NPR anchor cable. After the implementation of this new support scheme, the ratio of steel arch replacement in the K1738–K1813 section was zero. Fig.18 presents how effective the NPR scheme was for the surrounding rock support of No.2 inclined shaft. Especially the left shoulder (Fig.18a) and the vault (Fig.18b) of the tunnel, at which, the deformation was relatively high when the original support scheme was adopted, the NPR support effect was remarkable. This practical engineering application demonstrated that the asymmetric NPR anchor cable support scheme could effectively control the high-magnitude deformation of the surrounding rock of the tunnel at high depth and achieve an ideal supporting effect.

6 Conclusions

In order to solve the high deformation problem in the construction of No. 2 inclined shaft, the physical model testing method was adopted to establish the tunnel model, with which, a new tunnel support scheme with NPR anchor cable as the core was studied and the reliability of the scheme was demonstrated through engineering application. The main conclusions were:

(1) A digital speckle analysis system was used to quantify the displacement of rock surrounding a tunnel. As an depth of the tunnel increased, the deformation of the surrounding rock gradually increased, while the asymmetric characteristics of deformation became apparent, with deformation reaching higher magnitude at the left spandrel of the tunnel compared to the vault or the right spandrel. No support was provided to the tunnel, while the layered surrounding rock sustained slipping and cracking, eventually collapsing from the left side of the tunnel. At the locations, at which, the tunnel was given asymmetric NPR support, the surrounding rock deformation was well controlled at all depths and an improved support effect was obtained.

(2) Micro-ground-stress sensors installed within the surrounding rock characterized the distribution and development of shear stress during the loading steps. The shear stress of the surrounding rock gradually increased as the burial depth increased, while it decreased as the distance from the tunnel excavation surface increased. In the tunnel without support, incidents of the value returned by the stress sensor dropping sharply occurred, mainly due to the destruction of the rock surrounding the tunnel. In contrast, the stress sensors in the tunnel supported with NPR anchor cables operated normally throughout experimentation, without abnormal stress phenomena occurrence.

(3) An asymmetric NPR anchor cable support scheme was proposed according to the study results of the similar model tests and the new scheme was used to conduct industrial tests on site at No. 2 inclined shaft. The support effect was analyzed based on on-site monitoring results. Deformation stability of the tunnel walls generally occurred over a period of 25 days to 30 days. The convergence value for every part of the tunnel was lower than 500 mm, which was within the controllable range. Consequently, NPR anchor cable could therefore effectively control the deformation of the initial support of the tunnel, while these results could be used as a reference for support design of similar engineering works.

Acknowledgements

References

Cao XP, Wei FP, Wang B, Liu ZY (2018) Experimental Research on the Reasonable Support Scheme of Soft Rock Tunnel with High Ground Stress. J Railw Eng Soc 35(7):65-71, 102. (In Chinese)
https://doi.org/10.3969/j.issn.1006-2106.2018.07.012

Chen Z, He C, Wu D, et al. (2017) Fracture evolution and energy mechanism of deep-buried carbonaceous slate. Acta Geotech 12(6):1243-1260.
https://doi.org/10.1007/s11440-017-0606-5

Elizalde C, Griffith WA, Miller T (2016) Thrust fault nucleation due to heterogeneous bedding plane slip: Evidence from an Ohio coal mine. Eng Geol 206: 1-17.
https://doi.org/10.1016/j.enggeo.2016.03.001

Gong WL, Gong YX, Long AF (2013) Multi-filter analysis of infrared images from the excavation experiment in horizontally stratified rocks. Infrared Phys Technol 56(2):57–68.
https://doi.org/10.1016/j.infrared.2012.10.001

Gong WL, Peng Y, He MC, et al. (2015) Thermal image and spectral characterization of roadway failure process in geologically 45° inclined rocks. Tunn Undergr Space Technol 49:156-173.
https://doi.org/10.1016/j.tust.2015.04.011

He MC, Gong WL, Wang J, et al. (2014) Development of a novel energy-absorbing bolt with extraordinarily large elongation and constant resistance. Int J Rock Mech Min Sci 67:29-42.
https://doi.org/10.1016/j.ijrmms.2014.01.007

He MC (2011) Physical modeling of an underground roadway excavation in geologically 45° inclined rock using infrared thermography. Eng Geol 121(3-4):165-176.
https://doi.org/10.1016/j.enggeo.2010.12.001

Hisatake M, Ohno S (2008) Effects of pipe roof supports and the excavation method on the displacements above a tunnel face. Tunn Undergr Space Technol 23(2):120-127.
https://doi.org/10.1016/j.tust.2007.02.002

Jeon S, Kim J, Seo Y, et al. (2004) Effect of a fault and weak plane on the stability of a tunnel in rock-a scaled model test and numerical analysis. Int J Rock Mech Min Sci 41(3):486-0.
https://doi.org/10.1016/j.ijrmms.2004.03.115

Kang Y, Liu Q, Xi H, et al. (2018) Improved compound support system for coal mine tunnels in densely faulted zones: A case study of China's Huainan coal field. Eng Geol:

S0013795217313595.
https://doi.org/10.1016/j.enggeo.2018.04.006

Khorasani E, Amini M, Hossaini MF, et al. (2019) Statistical analysis of bimslope stability using physical and numerical models. Eng Geol 254: 13-24.
https://doi.org/10.1016/j.enggeo.2019.03.023

Kimura F, Okabayashi N, Kawamoto T (1987) Tunnelling through squeezing rock in two large fault zones of the Enasan Tunnel II. Rock Mech Rock Eng 20(3):151-166.
https://doi.org/10.1016/0148-9062(88)92988-9

Kulasingam R, Malvick EJ, Boulanger RW, et al. (2004) Strength Loss and Localization at Silt Interlayers in Slopes of Liquefied Sand. J Geotech Geoenviron Eng 130(11):1192-1202.
https://doi.org/10.1061/(ASCE)1090-0241(2004)130:11(1192)

Li SC, Zhou ZQ, Li LP, et al. (2013) Risk assessment of water inrush in karst tunnels based on attribute synthetic evaluation system. Tunn Undergr Space Technol 38:50-58.
https://doi.org/10.1016/j.tust.2013.05.001

Li SC, Wang Q, Wang HT, et al. (2015) Model test study on surrounding rock deformation and failure mechanisms of deep roadways with thick top coal. Tunn Undergr Space Technol 47:52-63.
https://doi.org/10.1016/j.tust.2014.12.013

Lin P, Liu X, Zhou W, et al. (2015) Cracking, stability and slope reinforcement analysis relating to the Jinping dam based on a geomechanical model test. Arab J Geosci 8(7):4393-4410.
https://doi.org/10.1007/s12517-014-1529-1

Lin P, Liu H, Zhou W (2015) Experimental study on failure behaviour of deep tunnels under high in-situ stresses. Tunn Undergr Space Technol 46:28-45.
https://doi.org/10.1016/j.tust.2014.10.009

Ma SP, Jin GC, Pan YS (2002) Deformation measurement method for rock materials based on natural speckle pattern. Chinese Journal of Rock Mech Rock Eng 21(6):792-796.
https://doi.org/10.2753/CSH0009-4633350347

Marinos V, Goricki A, Malandrakis E (2018) Determining the principles of tunnel support based on the engineering geological behaviour types: example of a tunnel in tectonically disturbed heterogeneous rock in Serbia. Bull Eng Geol Environ 78(4): 2887-2902.
https://doi.org/10.1007/s10064-018-1277-7

Merlini D, Stocker D, Falanesca M, et al. (2018) The Ceneri Base Tunnel: Construction Experience with the Southern Portion of the Flat Railway Line Crossing the Swiss Alps. Engineering 4(2):235-248.
https://doi.org/10.1016/j.eng.2017.09.004

Miwa M, Ogasawara M (2005) Tunnelling through an embankment using all ground fasten method. Tunn Undergr Space Technol 20(2):121-127.
https://doi.org/10.1016/j.tust.2003.12.001

Oreste PP, Pella D (1997) Modelling progressive hardening of shotcrete in convergence-confinement approach to tunnel design. Tunn Undergr Space Technol 12(3):425-431.
https://doi.org/10.1016/S0886-7798(97)00033-3

Ortlepp WD, Stacey TR (1998) Performance of tunnel support under large deformation static and dynamic loading. Tunn Undergr Space Technol 13(1):15-21.
https://doi.org/10.1016/S0886-7798(98)00022-4

Rui P, Qi W, Bei J, et al. (2019) Model test on failure and control mechanism of surrounding rocks in tunnels with super large sections. Arab J Geosci 12: 687.
https://doi.org/10.1007/s12517-019-4863-5

Simona R (2013) Analytical approach of the tunnel face effect on the rock-support interface in viscoelastic rock mass. American Institute of Physics 1558: 1354-1358.
https://doi.org/10.1063/1.4825764

Sun XM, Chen F, He MC, et al. (2017) Physical modeling of floor heave for the deep-buried roadway excavated in ten degree inclined strata using infrared thermal imaging technology. Tunn Undergr Space Technol 63: 228-243.
https://doi.org/10.1016/j.tust.2016.12.018

Sun XM, Chen F, Miao C, et al. (2018) Physical modeling of deformation failure mechanism of surrounding rocks for the deep-buried tunnel in soft rock strata during the excavation. Tunn Undergr Space Technol 74:247-261.
https://doi.org/10.1016/j.tust.2018.01.022

Tian HG, Chen WZ, Tan XJ, et al. (2011) Study of Reasonable Support Scheme for Soft Rock Tunnel in High Geostress Zone. Chin J Rock Mech Eng (11): 2285-2292. (In Chinese)
https://doi.org/10.1097/RLU.0b013e3181f49ac7

Wang SR, Xiao HG, Zou ZS, et al. (2019) Mechanical performances of transverse rib bar during pull-out test. Int J Appl Mech, Article ID 1950048, 11(5): 1-15.
https://doi.org/10.1142/S1758825119500480

Wang YL, Tan ZS (2012) Study on Structure Failure and Preventive Measures against Collapse of Muzhailing Tunnel in Slate. Rock Soil Mech 33 (Supp. 2): 263-268. (In Chinese)
https://doi.org/10.16285/j.rsm.2012.s2.028

Zhang DH, Liu SH, Ren SQ (2014) Research on selection of steel and steel grid for tunnel support in soft rock with high geostress. Chin J Rock Mech Eng 11:2258-2266. (In Chinese)
https://doi.org/10.13722/j.cnki.jrme.2014.11.010

Zhang JH, Chen ZY, Wang XG (2007) Centrifuge Modeling of Rock Slopes Susceptible to Block Toppling. Rock Mech Rock Eng 40(4):363-382.
https://doi.org/10.1007/s00603-006-0112-9

Zhang ZG, Zhang CP, Ma BB, et al. (2018) Physical model test and numerical simulation for anchor cable reinforcements of existing tunnel under action of landslide. Rock Soil Mech 39:No. 296(S1):60-69. (In Chinese)
https://doi.org/10.16285/j.rsm.2018.0625